Progress In Electromagnetics Research, PIER 103, 153–168, 2010

CHANNEL-RANKED BEAMFORMER FOR THE EARLY DETECTION OF BREAST CANCER

M. O'Halloran, M. Glavin, and E. Jones †

College of Engineering and Informatics
National University of Ireland Galway
University Road, Galway, Ireland

Abstract—Confocal Microwave Imaging (CMI) for the early detection of breast cancer is based on several assumptions regarding the dielectric properties of normal and malignant breast tissue. One of these assumptions is that the breast is primarily dielectrically homogeneous, and that the propagation, attenuation and phase characteristics of normal breast tissue allows for the constructive addition of the Ultra Wideband (UWB) returns from dielectric scatterers within the breast. However, recent studies by Lazebnik et al. have highlighted a very significant dielectric contrast between normal adipose and fibroglandular tissue within the breast. This dielectric heterogeneity presents a considerably more challenging imaging scenario, where constructive addition of the UWB returns, and therefore tumor detection, is much more difficult. In a dielectrically homogeneous breast, each additional beamformed backscattered signal adds coherently with existing signals, resulting in an improved image of any dielectric scatterers present. However, in a dielectrically heterogeneous breast, signals with a longer propagation distance are more likely to encounter heterogeneity and therefore are more prone to incoherent addition, reducing the overall quality of the breast image. In this paper, a novel beamforming algorithm is described, which gives extra weighting to signals with shorter propagation distances to create an improved image of the breast. The beamformer is shown to provide improved images of more dielectrically heterogeneous breasts than the traditional delay and sum beamformer from which it is derived.

Corresponding author: M. O'Halloran (martin.ohalloran@gmail.com).
† All the authors are also with Bioelectronics Research Cluster, National Centre for Biomedical Engineering Science (NCBES), National University of Ireland Galway, University Road, Galway, Ireland.

1. INTRODUCTION

More than 40,000 women die annually in the United States from breast cancer, making it the leading cause of death in American women. Worldwide, the incidence of breast cancer has increased by 0.5% annually, with 1.35 to 1.45 million new cases projected by 2010 [1]. X-ray mammography, coupled with comprehensive physical examinations and regular self-examinations, is currently the most effective screening method for the detection of breast cancer. However, the limitations of X-ray mammography in terms of imaging radiographically dense glandular tissue, especially common amongst younger women, motivate the development of alternate breast imaging modalities.

Several microwave breast imaging techniques have been developed in the last ten years. The physical basis for microwave imaging is the significant dielectric contrast between normal and malignant breast tissue that exists at microwave frequencies. Three alternative active microwave imaging techniques are under development, Hybrid Microwave-Induced Acoustic imaging [2–4], Microwave Tomography [5–10] and Ultra-Wideband (UWB) Radar imaging [11–21].

Ultra-Wideband (UWB) Radar imaging, as proposed by Hagness et al. [11], uses reflected UWB signals to determine the location of microwave scatterers within the breast. The Confocal Microwave Imaging (CMI) approach involves illuminating the breast with a UWB pulse, recording the backscattered signals and then using these signals to identify and locate significant dielectric scatterers within the breast. Regions of high energy within the resultant images may suggest the presence of cancerous tissue due to the dielectric contrast that exists between normal and cancerous tissue. The CMI approach is based on several assumptions regarding the dielectric properties of normal and cancerous breast tissue. Two of the most important assumptions are that the breast is primarily dielectrically homogeneous and consequently that the dielectric properties of normal tissue allow for coherent addition of the UWB backscattered signals.

However, a recent study of the dielectric properties of adipose, fibroglandular and cancerous breast tissue has highlighted the dielectric heterogeneity of normal breast tissue [22, 23]. Significantly, rather than the dielectric properties of normal breast tissue being homogeneous, Lazebnik et al. found a very significant dielectric contrast between adipose and fibroglandular tissue within the breast. The dielectric properties of adipose tissue was found to be lower than any previously published data for normal tissue. Conversely, the dielectric properties of fibroglandular tissue was found to be significantly higher than any

previously published data for normal breast tissue. This heterogeneity of normal breast tissue had been considerably underestimated in more historical studies, and the difficultly this presents to existing data-independent beamformers has been examined by the authors previously [24].

In this paper, a novel channel-ranked beamformer is presented which rewards signals with a shorter propagation distance in the image creation process. Because these signals have a shorter propagation path, the error between the assumed and actual channel model is less, and therefore coherent addition is made easier. The performance of the channel-ranked beamformer, in comparison to the delay and sum beamformer, is examined and evaluated with respect to several performance metrics. The remainder of the paper is organized as follows: Section 2 will review the recently-established dielectric heterogeneity of normal breast tissue; Section 3 will describe the channel-ranked beamformer; Section 4 will describe the test procedure and corresponding results; Finally, the conclusions and suggestions for future work are detailed in Section 5.

2. DIELECTRIC HETEROGENEITY OF NORMAL BREAST TISSUE

The dielectric properties (and heterogeneity) have been comprehensively examined previously [24, 25], and are summarised here for completeness.

Many of the historical studies examining the dielectric properties of breast tissue have tended to focus on the dielectric contrast between normal breast tissue (including both adipose and fibroglandular tissue) and cancerous tissue, rather than distinguishing between types of normal tissue and examining their respective dielectric properties in isolation. Chaudhary [26], Surowiec [27] and Joines et al. [28] all measured the dielectric properties of normal and cancerous breast tissues from 3 MHz and 3 GHz, 20 KHz to 100 MHz, and 50 MHz to 900 MHz respectively. Chaudhary found a significant dielectric contrast between normal and malignant tissue of $4.7:1$ for conductivity and $5:1$ for relative permittivity). Similarly, Joines found a contrast ratio of $3.8:1$ for conductivity and $6.4:1$ for relative permittivity. Surowiec found that the tissue at the infiltrating edge of the tumor had increased dielectric properties, suggesting that even quite small tumors could still induce significant microwave backscattering. While these studies established a significant dielectric contrast between normal and cancerous tissue, but did not examine the dielectric contrast between adipose and fibroglandular tissue.

One of the first dielectric studies to suggest that the breast may be more dielectrically heterogeneous was completed by Campbell and Land [29]. They measured the complex permittivity of female breast tissue at 3.2 GHz, and while once again noting a significant dielectric contrast between normal and cancerous tissue, they also suggested that the range of dielectric properties of normal tissue was much greater than established in previous studies. The heterogeneity of normal breast tissue was further confirmed by Meaney et al. [30] who noted that the average permittivity values of normal tissue at 900 MHz were significantly higher than those previously published in Joines et al.'s *ex vivo* study [28]. Meaney et al. suggested that breasts with a greater concentration of dense fibroglandular tissue tended to have higher average permittivity values than less dense breasts. Finally, one of the most comprehensive examinations of the dielectric properties of normal breast tissue, was undertaken by Lazebnik et al. [22]. The key attribute of Lazebnik et al.'s first study was the histological categorisation of the tissue samples. Each sample under consideration was quantified in terms of the percentage of adipose, glandular and fibroglandular tissue present in the sample. These results of Lazebnik's study can be effectively summarised as follows:

(i) Adipose tissue has much lower dielectric properties than previously assumed.

(ii) Conversely, fibroglandular tissue has much higher dielectric properties than previously thought.

(iii) The dielectric heterogeneity of normal breast tissue was previously significantly underestimated.

The effect of this dielectric heterogeneity is very significant. The performance and robustness of both UWB beamforming algorithms is highly dependent on the coherence of the backscattered signals from the tumor after time-alignment, and therefore their effectiveness is markedly reduced where there is a significant difference between the assumed homogenous channel model and the actual heterogeneous breast [24]. This prompts the development of more sophisticated beamformers to compensate for the more challenging imaging environment of the dielectrically heterogeneous breast.

3. CHANNEL-RANKED BEAMFORMER

The aim of the beamforming algorithm is to spatially focus the recorded signals to create an image of any scatterers present within the breast [31]. An effective beamforming algorithm must clearly identify the presence and location of any tumor while suppressing

clutter due to the normal heterogeneity of breast tissue. The CMI approach is based on the delay-and-sum beamformer, which time-shifts and sums recorded backscattered signals to create a synthetic focal point within the breast [11, 17, 32]. The energy at this synthetic focal point is measured, and by varying the position of the synthetic focal point within the breast an energy profile of the breast can be created. Regions of high energy within the resultant image may suggest the presence of cancerous tissue. However, rather than using all multistatic signals to create the image, the channel-select beamformer only uses channels which have a propagation distance less than a certain predetermined threshold. Since these signals have a shorter propagation path, the error between the actual heterogeneous breast channel and the beamformers assumed propagation channel is much less for these signals.

Consider a planar array of antennas spread across a naturally flattened breast with the patient lying in the supine position. Within the breast, consider a voxel of interest r_0, as shown in Figure 1. For each antenna transmission, the propagation distance between the transmitting antenna, the voxel r_0, and the receiving antenna is calculated. The distance is denoted by $d_{(i,j)}$ where i is the transmitting antenna index and j is the corresponding receiving antenna index. For multistatic signals, the distance $d_{(i,j)}$ is defined as:

$$d_{(i,j)} = d_{tat} + d_{tar} \tag{1}$$

where d_{tat} is the distance between the transmitting antenna and r_0 and d_{tar} is the distance between r_0 and the receiving antenna as shown in Figure 1. For the signal recorded at the transmitting antenna itself the distance is simply:

$$d_{(i,i)} = 2d_{tat} \tag{2}$$

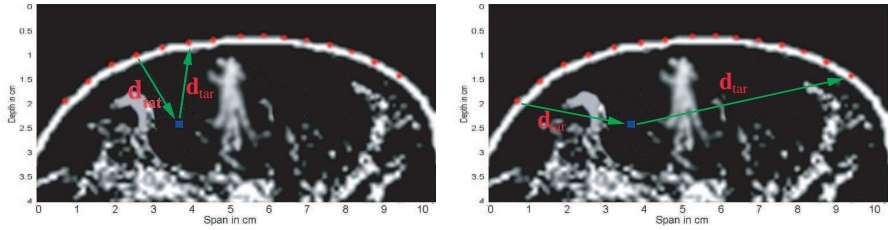

(a) (b)

Figure 1. Signals with a shorter propagation distance to the point r_0, as shown in (a), are given a greater weighting than signals with a longer propagation path, such as the signal shown in (b).

The round-trip time (in samples) to r_0, and back to the receiving antenna, is then calculated as follows:

$$T_{rt(i,j)} = \frac{d_{(i,j)}}{s} f_s \tag{3}$$

where f_s is the sampling frequency, and s is the average speed of propagation in breast tissue and is defined as follows:

$$s = \frac{c}{\sqrt{\epsilon_r}} \tag{4}$$

where ϵ_r is the relative permittivity of normal breast tissue at the centre frequency of the UWB input signal and c is the speed of light. Each of the signals is then delayed, to coarsely time-align all the responses from the candidate location as a pre-processing step to allow further processing to take place. The delay to be applied to each channel is defined as:

$$\tau_{(i,j)} = \max(T_{rt}) - T_{rt(i,j)} \tag{5}$$

Once the delay is applied to each channel, and the response from the scan location of interest coarsely aligned, $\max(T_{rt})$, the delay term is removed, to ignore energy from any interference or clutter present outside the time window of interest.

Each signal is then assigned a rank, $rank_{(i,j)}$, from 1 to N (N is the number of multistatic signals) based on its round-trip distance from the point of interest, r_0, with the signal with the shortest propagation distance assigned a rank of 1. A weighting factor is then applied based on this ranking, and is calculated as follows:

$$w_{(i,j)} = \frac{N - rank_{(i,j)}}{N(N+1)/2} \tag{6}$$

This formulation gives greater weighting to signals with shorter propagation distances. However, it also requires that the sum of the weights is always equal to 1, ensuring that reflections from scatterers deeper within the breast, and with naturally longer propagation distances, are not penalised by the channel-ranked beamformer. The energy at the point of interest is then calculated as:

$$I(\mathbf{r_0}) = \int_0^h \left[\sum_{i=1}^{N} \sum_{j=1}^{N} w_{(i,j)} S_{(i,j)}(t - \tau_{(i,j)}) \right]^2 dt \tag{7}$$

where $S_{(i,j)}$ is the backscattered signal at antenna j due to the transmitted signal from antenna i, and h is the window containing the backscattered response. As described by Bond et al. [33], if the tumor is large, the duration of the backscattered tumor response will be

greater, and so a larger window would be more appropriate in this case. However, since we are concerned with the detection of small tumors, a smaller temporal window is chosen to more effectively determine the presence of early-stage cancers. While this may lessen somewhat the strength of the return from larger tumors compared to background clutter, these large tumors inherently provide a much stronger response and so detection of these tumors should not be problematic. The synthetic focus is then scanned throughout the breast in increments of 1 mm^2 (depth and span). The energy is converted to an appropriate pixel intensity and an image of the breast is created.

4. TESTING AND RESULTS

4.1. 2D FDTD Models

A 2D FDTD breast model was developed, based on a naturally flattened breast from a patient lying in the supine position. Therefore, in two dimensions, a sagittal slice of breast is considered with a conformal antenna array placed close to the skin. The antenna array consists of 14 elements modeled as electric-current sources, and are equally spaced on the surface of the skin along the horizontal span-axis from 1 cm to 9 cm. The antenna array is backed by a synthetic material matching the dielectric properties of skin. The adipose/fibroglandular tissue distribution within the breast is established by linearly mapping the regions of adipose and fibroglandular tissue from a high resolution T2 weighted MR image to the FDTD grid, as previously used by Li et al. [17]. The lighter regions within the breast represented fibroglandular tissue, while the darker regions represented adipose tissue. A simple thresholding algorithm was applied to the MRI scan to differentiate between the different regions of tissue, and then a linear transformation algorithm was used to map the tissue distribution in the MRI scan to the FDTD grid. This method was chosen since it preserved the highly correlated nature of fibroglandular tissue distribution in the breast, as opposed to the other methods that model the variance of dielectric properties as being randomly distributed.

In this model, there are considerable regions of fibroglandular tissue, but also regions of adipose tissue where no fibroglandular tissue is present, as shown in Figure 2. The FDTD grid resolution, dx, is 0.5 mm and the time step dt is defined as 0.833 ps ($dt = \frac{dx}{2c}$). A specific location within the FDTD model is defined as follows: (*depth* cm, *span* cm). A 15 mm, 10 mm and 6 mm tumor is artificially introduced at nine different locations within the model: (1.5, 3.5), (2.0, 3.5), (2.5, 3.5), (1.5, 4.0), (2.0, 4.0), (2.5, 4.0), (1.5, 6.5), (2.0, 6.5) and (3.0, 6.5).

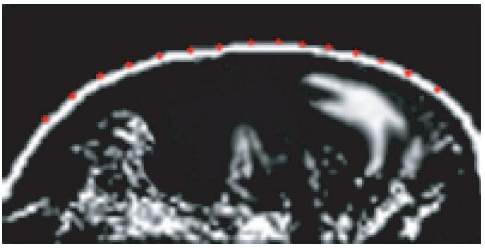

Figure 2. FDTD model of the breast. The lighter regions of the breast represent fibroglandular tissue, while the darker regions are representative of adipose tissue. The locations of the antennas on the skin surface are shown in red, while the various tumor locations are shown in blue.

Table 1. Debye parameters for the FDTD model and dielectric properties of each tissue at the centre frequency of the input pulse.

Tissue	ϵ_r	χ_1	σ	t_0 (ps)	Relative Perm.	Cond. (S/m)
Skin	15.63	8.2	0.82	12.6	21.65	2.35
Tumor	7	47	0.15	7	49.2	6.1
Adipose (Medium)	3.20	1.65	0.035	16	4.30	0.38
Fibroglandular (Medium)	11.2	38	0.738	12	39.65	7.65

Since there are 14 antenna array elements, this results in 196 recorded multistatic signals. Before further processing, the signals are downsampled from 1200 GHz (the time step in the FDTD simulation) to 50 GHz. The input signal is a 150-ps differentiated Gaussian pulse, with a centre frequency of 7.5 GHz and a -3 dB bandwidth of 9 GHz. An idealized artifact removal algorithm, as previously described by Bond et al. [33] is used to remove the input signal and the reflection from the skin-breast interface. The artifact to be removed is established by measuring the backscattered signals from the first homogeneous FDTD model with no tumor present. These signals are then subtracted channel-by-channel from the with-tumor responses. Finally, since the input signal is a differentiated Gaussian pulse with a zero crossing at its centre point, the backscattered signal from any dielectric scatterer would also have a zero crossing at its centre point. In order to overcome this, the signals are integrated to produce a maximum at the centre point.

The Debye parameters for skin are chosen to fit published data by Gabriel et al. [34, 35], while the Debye parameters for malignant tissue are those used by Bond et al. [33]. The dielectric properties of adipose and fibroglandular tissue used in the FDTD models are based on Lazebnik et al.'s recent publications [22, 23]. The Debye parameters for each type of tissue, along with the permittivity and conductivity at the centre frequency, are shown in Table 1.

4.2. Metrics

In order to compare the robustness and performance of the channel-ranked and delay and sum beamformer, two specific metrics are used:

- Signal-to-Clutter Ratio within-breast (SCR) [13, 36]
- Signal-to-Mean Ratio (SMR) [37, 38]

The SCR within-breast compares the maximum tumor response to the maximum clutter response in the same image. To obtain the value of the maximum clutter, the maximum pixel value of the image is found, excluding the area which includes the tumor peak response up to twice the extent of the FWHM response of the tumor itself [13, 36]. The SMR compares the maximum tumor response with the mean response of the different tissues across the breast in the same image of backscattered energy [37, 38].

4.3. Results

Twenty seven different FDTD simulations were completed, with three different-sized tumors positioned at nine different locations within the breast. Both the delay and sum and channel-ranked beamformer were applied to each set of backscattered signals. The SCR and SMR ratio were calculated for each simulation, and are shown in Table 2.

The channel-ranked beamformer gives extra weighting to signals with a shorter propagation path (and therefore, signals which have in general encountered less heterogeneity) to identify the presence of significant dielectric scatterers within the breast. In most cases, the channel-ranked beamformer offers a significant improvement in SCR over the delay and sum beamformer, as much as 6.63 dB in one case (15 mm at location (2.5, 4.0)), and with an average improvement of 2.56 dB over all tests. Also, the average increase in SMR provided by the channel-ranked beamformer is 1.35 dB.

Examining both the SCR and SMR in Table 2, the improvement (in SCR and SMR) offered by the channel-ranked beamformer generally increases with tumor depth. This is due to the fact that the level of heterogeneity encountered by the multistatic signals also

Table 2. SCR and SMR for both the delay and sum and Channel-Ranked beamformer for a 15 mm, 10 mm and 6 mm tumor at nine different locations within the breast model.

15 mm										
Metric	Beamformer	(1.5, 3.5)	(2.0, 3.5)	(2.5, 3.5)	(1.5, 4.0)	(2.0, 4.0)	(2.5, 4.0)	(1.5, 6.5)	(2.0, 6.5)	(3.0, 6.5)
SCR	DAS	5.1347	16.1366	12.9460	5.8537	18.7071	14.4607	7.80	−3.299	−13.55
(dB)	CRDAS	6.8220	18.2680	18.0533	5.0615	18.1784	21.0995	12.45	0.3788	−8.03
SMR	DAS	11.3467	22.2340	20.0451	10.0869	22.3294	21.0445	20.87	6.58	−5.061
(dB)	CRDAS	10.8147	24.8117	23.1713	12.1939	23.4970	25.0972	23.40	9.011	0.1913
10 mm										
Metric	Beamformer	(1.5, 3.5)	(2.0, 3.5)	(2.5, 3.5)	(1.5, 4.0)	(2.0, 4.0)	(2.5, 4.0)	(1.5, 6.5)	(2.0, 6.5)	(3.0, 6.5)
SCR	DAS	5.9020	14.4053	8.5537	8.1642	17.7424	7.6653	8.35	5.62	−10.14
(dB)	CRDAS	2.7389	18.7947	9.5248	7.9537	21.1011	13.9867	10.955	7.9309	−11.11
SMR	DAS	11.8681	21.6408	14.8871	12.5296	21.8058	13.1930	19.42	16.13	−1.825
(dB)	CRDAS	8.0009	24.7023	12.7299	13.3128	24.6046	16.6082	20.72	17.13	−3.585
6 mm										
Metric	Beamformer	(1.5, 3.5)	(2.0, 3.5)	(2.5, 3.5)	(1.5, 4.0)	(2.0, 4.0)	(2.5, 4.0)	(1.5, 6.5)	(2.0, 6.5)	(3.0, 6.5)
SCR	DAS	14.8887	11.3187	0.8141	17.2370	12.7167	−5.3088	2.32	6.3094	−9.45
(dB)	CRDAS	15.6469	16.2896	5.6078	16.8563	19.3139	−4.0116	4.30	8.39	−5.95
SMR	DAS	18.9154	18.5840	7.6667	20.2940	19.7227	−0.7890	12.26	15.09	−0.84
(dB)	CRDAS	19.5828	20.5336	9.3140	20.1503	22.8627	−2.3277	12.52	16.08	1.1142

increases with depth, making the imaging problem more difficult and making the requirement for intelligent channel-weighting even more important.

Furthermore, Table 2 indicates that the channel-ranked beamformer significantly outperforms the delay and sum beamformer in the case of the 6 mm tumour. This is due to the fact that the smaller tumor provides a much more difficult imaging scenario, where the imaging difficulties associated with dielectric heterogeneity are more apparent. The beamformer rewards the channels with shorter propagation distance which, due to the fact that they have typically encountered less dielectric heterogeneity, tend to add more coherently at the tumor site, resulting in a considerably improved image of smaller tumors.

The channel-ranked beamformer also offers a significant improvement in resolution compared to the delay and sum beamformer, illustrated in the resultant images, where resolution is defined as the ability to differentiate between two adjacent scatterers within the breast. A tumor is positioned at location (1.5, 3.0) within the breast model and both the delay and sum (Figure 3(a)) and channel-ranked beamformer (Figure 3(b)) are applied to the backscattered signals. The tumor is located close to a region of fibroglandular tissue, which itself is a significant dielectric scatterer. In the resultant delay and sum image, it's quite difficult to differentiate between the fibroglandular scatterer located at (1.5, 2.5) and the tumor at (1.5, 3.0). However, the two individual scatterers are much more clearly visible in the channel-ranked beamformer image. This is further illustrated in Figure 4, where a

tumor is located at (2.5, 3.5). Once again, each individual scatterer is more easily visible in the channel-ranked image than in the corresponding delay and sum image.

Therefore, the overall affect of the channel-ranked beamformer is a significantly improved image compared to the existing delay and sum beamformer, where dielectric scatterers (both cancerous and non-cancerous fibroglandular tissue) are more clearly visible against the cluttered background.

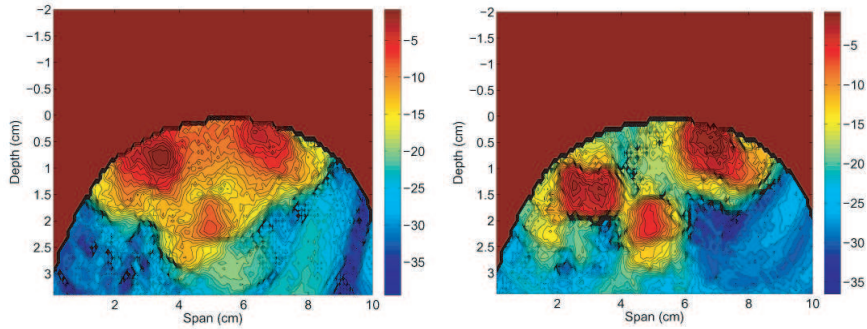

Figure 3. Comparison of delay and sum, (a) and channelranked beamformer, (b), with a tumor located at (1.5, 3.0). The channel-ranked beamformer offers significant improvement in resolution compared to the delay and sum beamformer, making it much easier to differentiate between adjacent dielectric scatterers.

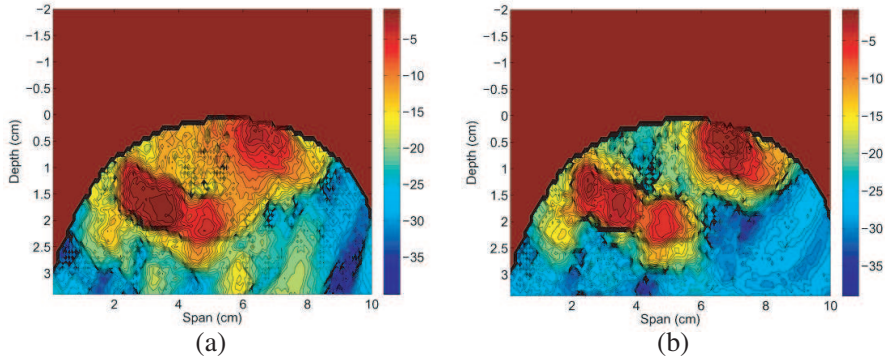

Figure 4. Delay and Sum and Channel-ranked beamformer image of a tumor located at (1.5, 2.5). Each individual scatterer is visible in the channel-ranked image, as opposed to the delay and sum image where the scatterer responses overlap significantly.

5. CONCLUSIONS AND FUTURE WORK

The Confocal Microwave Imaging approach is based on the assumption that the breast is primarily homogeneous and the dielectric properties of the breast allow for the coherent addition of the reflected UWB signals. If this assumption was accurate, each UWB multistatic signal would add coherently at the tumor location and provide for an improved image in terms of SCR and SMR. However, recent research by Lazebnik et al. has shown that the dielectric heterogeneity of normal breast tissue had previously been significantly underestimated, presenting a much more challenging imaging scenario. In this paper, a novel channel-ranked beamformer was described and tested. The beamformer gives extra weighting to channels with shorter propagation distances to image the breast. These signals have typically encountered less heterogeneity and therefore the error between the assumed homogeneous propagation model and the actual propagation path has less of an effect. The channel-ranked beamformer has been comprehensively tested on a dielectrically heterogeneous breast model and has been shown to significantly outperform the delay and sum beamformer in terms of SCR and SMR, across a range of tumor locations and sizes (an average of 2.44 and 1.25 dB respectively, with individual improvements as large as 6.6 dB). The channel-ranked has also been shown to provide improved resolution, making it possible to differentiate between two adjacent scatterers. Future work will concentrate on differentiating between the regions of cancerous and non-cancerous (fibroglandular) regions in the resultant UWB images.

ACKNOWLEDGMENT

This work is supported by Science Foundation Ireland (SFI) under grant number 07/RFP/ENEF420.

REFERENCES

1. Nass, S. L., I. C. Henderson, and J. C. Lashof, *Mammography and Beyond: Developing Technologies for the Early Detection of Breast Cancer*, National Academy Press, 2001.
2. Wang, L., X. Zhao, H. Sun, and G. Ku, "Microwave-induced acoustic imaging of biological tissues," *Rev. Sci. Instrum.*, Vol. 70, No. 9, 3744–3748, 1991.
3. Li, D., P. M. Meaney, T. Raynolds, S. A. Pendergrass, M. W. Fanning, and K. D. Paulsen, "Parallel-detection microwave

spectroscopy system for breast cancer imaging," *Rev. Sci. Instrum.*, Vol. 75, No. 7, 2305–2313, 2004.

4. Kruger, R. A., K. D. Miller, H. E. Reynolds, W. L. Kiser, D. R. Reinecke, and G. A. Kruger, "Breast cancer in vivo: Contrast enhancement with thermoacoustic CT at 434 MHz — Feasibility study," *Radiology*, Vol. 216, No. 1, 279–283, 2000.
5. Bulyshev, A., S. Y. Semenov, A. E. Souvorov, R. H. Svenson, A. G. Nazorov, Y. E. Sizov, and G. P. Tatsis, "Computational modeling of three-dimensional microwave tomography of breast cancer," *IEEE Trans. Biomed. Eng.*, Vol. 48, No. 9, 1053–1056, Sep. 2001.
6. Meaney, P. M., M. W. Fanning, D. Li, S. P. Poplack, and K. D. Paulsen, "A clinical prototype for active microwave imaging of the breast," *IEEE Trans. Microwave Theory Tech.*, Vol. 48, No. 11, 1841–1853, Nov. 2000.
7. Meaney, P. M., K. D. Paulsen, J. T. Chang, M. W. Fanning, and A. Hartov, "Nonactive antenna compensation for fixed-array microwave imaging: Part II — Imaging results," *IEEE Trans. Med. Imag.*, Vol. 18, No. 6, 508–518, Jun. 1999.
8. Souvorov, A. E., A. E. Bulyshev, S. Y. Semenov, R. H. Svenson, and G. P. Tatis, "Two-dimensional analysis of a microwave flat antenna array for breast cancer tomography," *IEEE Trans. Microwave Theory Tech.*, Vol. 48, No. 8, 1413–1415, Aug. 2000.
9. Bulyshev, A. E., S. Y. Semenov, A. E. Souvorov, R. H. Svenson, A. G. Nazorov, Y. E. Sizov, and G. P. Tatsis, "Computational modeling of three-dimensional microwave tomography of breast cancer," *IEEE Trans. Biomed. Eng.*, Vol. 48, No. 9, 1053–1056, Sep. 2001.
10. Liu, Q. H., Z. Q. Zhang, T. Wang, J. A. Byran, G. A. Ybarra, L. W. Nolte, and W. T. Joines, "Active microwave imaging i — 2-d forward and inverse scattering methods," *IEEE Trans. Microwave Theory Tech.*, Vol. 50, No. 1, 123–133, Jan. 2002.
11. Hagness, S. C., A. Taflove, and J. E. Bridges, "Two-dimensional FDTD analysis of a pulsed microwave confocal system for breast cancer detection: Fixed-focus and antenna-array sensors," *IEEE Trans. Biomed. Eng.*, Vol. 45, No. 12, 1470–1479, 1998.
12. Hagness, S. C., "Three-dimensional FDTD analysis of a pulsed microwave confocal system for breast cancer detection: Design of an antennaarray element," *IEEE Trans. Antennas and Propagat.*, Vol. 47, No. 5, 783–791, May 1999.
13. Fear, E. C., X. Li, S. C. Hagness, and M. A. Stuchly, "Confocal microwave imaging for breast cancer detection: Localization of

tumors in three dimensions," *IEEE Trans. Biomed. Eng.*, Vol. 49, No. 8, 812–822, Aug. 2002.

14. Fear, E. C. and M. A. Stuchly, "Microwave system for breast tumor detection," *IEEE Microwave and Guided Wave Letters*, Vol. 9, No. 11, 470–472, Nov. 1999.
15. Fear, E. C., J. Sill, and M. A. Stuchly, "Experimental feasibility study of confocal microwave imaging for breast tumor detection," *IEEE Trans. Microwave Theory Tech.*, Vol. 51, No. 3, 887–892, Mar. 2003.
16. Fear, E., J. Sill, and M. Stuchly, "Microwave system for breast tumor detection: Experimental concept evaluation," *IEEE AP-S International Symposium and USNC/URSI Radio Science Meeting*, Vol. 1, 819–822, San Antonio, Texas, Jun. 2002.
17. Li, X. and S. C. Hagness, "A confocal microwave imaging algorithm for breast cancer detection," *IEEE Microwave and Wireless Components Letters*, Vol. 11, No. 3, 130–132, 2001.
18. Li, X., E. J. Bond, B. D. V. Veen, and S. C. Hagness, "An overview of ultra-wideband microwave imaging via space-time beamforming for early-stage breast-cancer detection," *IEEE Antennas and Propagation Magazine*, Vol. 47, No. 1, 19–34, Feb. 2005.
19. Craddock, I. J., R. Nilavalan, J. Leendertz, A. Preece, and R. Benjamin, "Experimental investigation of real aperture synthetically organised radar for breast cancer detection," *IEEE AP-S International Symposium*, Washington, DC, 2005.
20. Hernandez-Lopez, M., M. Quintillan-Gonzalez, S. Garcia, A. Bretones, and R. Martin, "A rotating array of antennas for confocal microwave breast imaging," *Microw. Opt. Technol. Lett.*, Vol. 39, No. 4, 307–311, Nov. 2003.
21. De Rodriguez, M., M. Vera-Isasa, and V. S. del Rio, "3-D microwave breast tumor detection: Study of system performance," *IEEE Trans. Biomed. Eng.*, Vol. 55, No. 12, 2772–2777, 2008.
22. Lazebnik, M., L. McCartney, D. Popovic, C. B. Watkins, M. J. Lindstrom, J. Harter, S. Sewall, A. Magliocco, J. H. Booske, M. Okoniewski, and S. C. Hagness, "A large-scale study of the ultrawideband microwave dielectric properties of normal breast tissue obtained from reduction surgeries," *Phys. Med. Biol.*, Vol. 52, 2637–2656, 2007.
23. Lazebnik, M., D. Popovic, L. McCartney, C. B. Watkins, M. J. Lindstrom, J. Harter, S. Sewall, T. Ogilvie, A. Magliocco, T. M. Breslin, W. Temple, D. Mew, J. H. Booske, M. Okoniewski, and S. C. Hagness, "A large-scale study of the ultrawideband microwave dielectric properties of normal, benign and malignant

breast tissues obtained from cancer surgeries," *Phys. Med. Biol.*, Vol. 52, 6093–6115, 2007.

24. O'Halloran, M., M. Glavin, and E. Jones, "Effects of fibroglandular tissue distribution on data-independent beamformering algorithms," *Progress In Electromagnetic Research*, PIER 97, 141–158, 2009.
25. O'Halloran, M., R. Conceicao, D. Byrne, M. Glavin, and E. Jones, "FDTD modeling of the breast: A review," *Progress In Electromagnetics Research B*, Vol. 18, 1–24, 2009.
26. Chaudhary, S. S., R. K. Mishra, A. Swarup, and J. M. Thomas, "Dielectric properties of normal and malignant human breast tissue at radiowave and microwave frequencies," *Indian J. Biochem. Biophys.*, Vol. 21, 76–79, 1984.
27. Surowiec, A. J., S. S. Stuchly, J. R. Barr, and A. Swarup, "Dielectric properties of breast carcinoma and the surrounding tissues," *IEEE Trans. Biomed. Eng.*, Vol. 35, No. 4, 257–263, Apr. 1988.
28. Joines, W. T., Y. Zhang, C. Li, and R. L. Jirtle, "The measured electrical properties of normal and malignant human tissues from 50 to 900 MHz," *Med. Phys.*, Vol. 21, No. 4, 547–550, Apr. 1994.
29. Campbell, A. M. and D. V. Land, "Dielectric properties of female human breast tissue measured in vitro at 3.2 GHz," *Phys. Med. Biol.*, Vol. 37, No. 1, 193–210, 1992.
30. Meaney, P. M., M. W. Fanning, D. Li, S. P. Poplack, and K. D. Paulsen, "A clinical prototype for active microwave imaging of the breast," *IEEE Trans. Microwave Theory Tech.*, Vol. 48, 1841–1853, 2000.
31. Haykin, S. and A. Steinhardt, *Adaptive Radar Detection and Estimation*, John Wiley and Sons, 1992.
32. Fear, E. C. and M. A. Stuchly, "Microwave detection of breast cancer," *IEEE Trans. Microwave Theory Tech.*, Vol. 48, No. 11, 1854–1863, Nov. 2000.
33. Bond, E. J., X. Li, S. C. Hagness, and B. D. V. Veen, "Microwave imaging via space-time beamforming for early detection of breast cancer," *IEEE Trans. Antennas and Propagat.*, Vol. 51, No. 8, 1690–1705, Aug. 2003.
34. Gabriel, C., S. Gabriel, and E. Corthout, "The dielectric properties of biological tissues: I. Literature survey," *Phys. Med. Biol.*, Vol. 41, 2231–2249, 1996.
35. Gabriel, S., R. W. Lau, and C. Gabriel, "The dielectric properties of biological tissues: II. Measurements in the frequency range

10 Hz to 20 GHz," *Phys. Med. Biol.*, Vol. 41, 2251–2269, 1996.

36. Fear, E. C. and M. Okoniewski, "Confocal microwave imaging for breast tumor detection: Application to a hemispherical breast model," *2002 IEEE MTT-S International Microwave Symposium Digest*, Vol. 3, 1759–1762, Seattle, WA, USA, 2002.
37. Klemm, M., I. J. Craddock, J. A. Leendertz, A. Preece, and R. Benjamin, "Improved delay-and-sum beamforming algorithm for breast cancer detection," *International Journal of Antennas and Propagation*, Vol. 2008, 2008.
38. Conceição, R. C., M. O'Halloran, M. Glavin, and E. Jones, "Antenna configurations for ultra wide band radar detection of breast cancer," *Progress in Biomedical Optics and Imaging*, Vol. 7169, San Jose, CA, Jan. 2009.